Phase Noise to Carrier Ratio in LC Oscillators

Qiuting Huang, *Senior Member, IEEE*

***Abstract*—An analysis is presented in this contribution to describe the steady-state amplitude of a CMOS LC Colpitts oscillator, as well as its response to small interferences. The problem of signal dependency of noise sources is also addressed. The general conclusions of the analysis are applicable to most LC oscillators. The procedure to perform a general analysis for an arbitrary LC oscillator is outlined. Controlled experiments are used to verify each important conclusion for the Colpitts analysis and implications on design are discussed.**

***Index Terms*—Class C operation of oscillator, Colpitts oscillator, dependence of noise to arrier ratio on the resonator quality factor in an oscillator, equivalent noise source in oscillators, LC oscillator, Leeson's model, noise sources in an oscillator, oscillation amplitude, oscillator, phase noise, phase-noise to carrier ratio, start-up of oscillation, voltage dependence of noise source in an oscillator.**

I. Introduction

THE IMPORTANCE of phase noise in oscillators in RF and other communications circuits has made it one of the most extensively studied subjects in electronics. Journal papers or books on phase noise in LC oscillators alone [1]–[13] can be found from each of the last six decades, the earliest one [1] being as old as 1938 and the latest ones as recent as 1998 [12], [13]. The fact that papers on LC oscillators (too numerous in the last 60 years to cite exhaustively) keep appearing, serves to underline the need still felt by many researchers to improve existing theories on phase noise further in terms of both rigor and insight.

Experimentally, the qualitative behavior of phase noise has been well known. An oscillator's output power spectrum consists of a peak at the carrier (main oscillation) angular frequency ω_o, surrounded by a noise skirt symmetrical to the carrier frequency. Although we restrict our discussion to LC oscillators in this paper, the oscillator noise skirt displays the following characteristics irrespective of the exact implementation.

1. The output noise spectral density is inversely proportional to the (square of) frequency offset from the carrier, except at very close to the carrier frequency, where the influence of up-converted flicker noise dominates or the presence of the strong carrier begins to limit measurement accuracy.
2. The same noise manifests itself in the time domain as jitter around the oscillation's zero-crossing points, which can only be interpreted as noise in the phase of the oscillation, rather than that superimposed on its waveform. Oscillator noise is therefore usually referred to as phase noise. The assumption of phase noise implies that the sideband spectrum above and below the carrier frequency must be equal in amplitude and opposite in sign.
3. It is widely believed [14] that doubling the quality factor of the LC tank roughly improves the oscillator's noise spectral density to carrier (N/C) ratio by 6 dB, although systematic experimental verification of such a belief is hard to find in open literature.

Because of Observation 3 above, the great majority of commercial RF oscillators today are implemented with high-quality inductors and capacitors outside the chip containing the active devices. At the same time, we witness widespread efforts in the integrated circuit research community to improve the quality of fully integrated inductors on silicon, especially in the last few years [14]–[28]. Despite the avalanche of research papers, the quality factor Q of on-chip inductors in standard CMOS and BJT technologies has hardly improved by a factor of two (from $Q \leq 3$ to $Q \leq 6$ at 1 GHz, or from $Q \leq 5$ to $Q \leq 10$ at 2 GHz) in the last ten years. The reported noise to carrier (N/C) ratio, however, varies by as much as 20 dB, for example, at 100 kHz offset from 1 GHz. The discrepancy underlines the need for us to understand better the factors other than the Q of the tank that may also affect N/C ratio strongly. Better models of phase noise are still needed.

For designers of electronic oscillators for communications, carrier amplitude (LO power), timing jitter or the N/C ratio at certain ranges of frequency offset, and power consumption are usually most important. They are therefore often interested in the following questions.

1. How does the carrier amplitude depend on the electrical parameters of the oscillator?
2. Why does an interference (white noise for example) that is often apparently added to the carrier in the circuit end up affecting only the phase of the oscillation? Why is the response to such an interference always inversely proportional to its frequency offset from the carrier, even in the apparent passband region of the passive resonator?
3. How does the N/C ratio depend on the electrical parameters of the oscillator? Can such dependence be described directly with the circuit parameters, rather than intermediate quantities such as the signal power consumed by the tank, the mean-squared voltage amplitude, or the noise factor of the oscillator?

For such designers, most existing models are incomplete because they either describe only noise and not the N/C ratio that is more important, or describe the N/C ratio via intermediate quantities such as the noise figure of the active device or power (amplitude) of the carrier signal. These intermediate quantities may in turn be functions of other electrical parameters of the oscillator.

Manuscript received March 11, 1999; revised December 12, 1999. This paper was recommended by Associate Editor J. Suykens.

The author is with the Integrated Systems Laboratory, Swiss Federal Institute of Technology (ETH), ETH-Zentrum, CH-8092 Zurich, Switzerland.

Publisher Item Identifier S 1057-7122(00)05505-7.

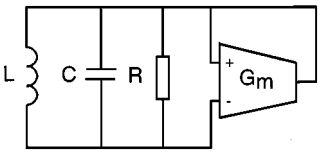

Fig. 1. Simple model used in typical linear analysis.

From the theoretical point of view, the rigor with which many popular phase noise models today are derived can still be improved to provide an insightful answer to Question 2 above. Since the analytical expressions of different models, incomplete as they are, do not always agree with one another, rigor in both theoretical derivation and experimental verification also remains the only way to sort the correct answer out. To appreciate the strengths and weaknesses of existing models, we can group the best-known papers (in electrical engineering journals at least) describing oscillator phase noise into four categories, according to whether the analysis is carried out in the frequency or time domain and whether noise input is assumed to be added to the carrier signal itself or the phase thereof [29].

Linear, frequency-domain analyses simply assume that noise is superimposed on the carrier and the transfer function from the noise source to the oscillator output is that of the resonator tank modified by the equivalent linear transconductance of the active device. Fig. 1 shows the equivalent circuit of the simplest case [11]. The *V–I* characteristic of a real active device, on the other hand, can generally be depicted as in Fig. 2, with a $\mathcal{N}$ shape serving as a necessary feature to limit the oscillation amplitude [30]. The negative slope representing the negative (trans)conductance required for startup is usually found in the middle. Since this *V–I* curve is usually highly nonlinear, the approaches used to obtain the equivalent linear transconductance (gm) have been different.

Earlier analyses [2] allow the equivalent gm to be quite different from the critical transconductance (g_{mc}) required to cancel the loss of the tank exactly. Such analyses result in models that generally predict a bandpass characteristic centered at the carrier frequency, flat at frequencies immediately adjacent to the carrier and rolling off at 6 dB per octave at higher offset frequencies. The corner between the two offset frequency ranges is typically of the order of the carrier frequency divided by the Q of the passive tank, which can be 10 MHz for a 1-GHz oscillator and a Q of 50. Such corner frequencies are not observed in practice. To fit to experimental results, later analyses [9], [11] assume that the transconductance (or gain) of the active device, seen by the noise signal, is exactly the same as that for the carrier, which in turn must be the same as that required to cancel the tank loss in steady state. The resulting equivalent circuit is an ideal zero-loss linear resonator. The inverse dependency on offset frequency is now present all the way to the carrier.

The problem with the use of the carrier's gm is that the latter is only a crude large-signal concept indicating the ratio between the fundamental component of a distorted output current of a transistor and the (sinusoidal) voltage applied to its input. The noise component, being a smaller signal at a different frequency and phase, does not traverse the nonlinear *V–I* curve in Fig. 2 in the same way as the carrier, even though it is superimposed on the latter. The distortion it experiences, or the average gm applicable, will therefore also be different from that of the carrier. Apart from predicting a noise response that is 6 dB too high at low-offset frequencies, linear analyses also suffer from the fundamental inability to predict the odd symmetry in output noise spectrum that is essential to modulation in phase.

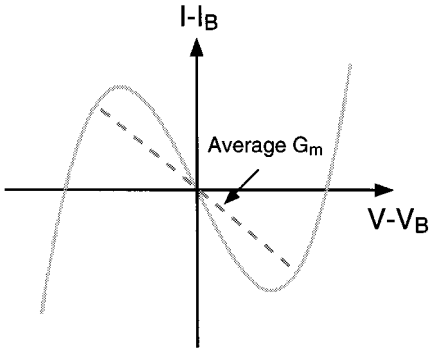

Fig. 2. Typical description of *V–I* characteristic of an active device and its average gm for a large signal. Practical transistors can be even more nonlinear.

Another way linear analysis is used in the frequency domain is to consider noise sources to be additive directly to the phase of the carrier [6], [7]. The result is best known as Leeson's model, which has become the most popular model for phase noise in the last 30 years. For white noise to be additive to the phase directly, however, it must be located at places where it can influence the frequency or phase-setting elements of the oscillator, such as the junction diodes (intentional or parasitic) in series or parallel with the main linear, passive tank. Since the phase (or frequency) shift caused by white noise on the reverse bias of a junction diode is solely determined by the C–V characteristic of the capacitor and its relative importance to other linear capacitors in the tank, the introduction of P_s (carrier power) into the input phase noise seems quite arbitrary. Numerical verifications with practical oscillators also show that noise levels associated with junction diodes are too low compared to the noise observed at the oscillator output, not least because good oscillators are designed to minimize the influence of parasitic diodes and the bias circuits of frequency-setting varactors usually have low-pass characteristics with cutoff frequencies well below the oscillation frequency.

In addition to Leeson's paper, there are analyses in the time domain that also assume noise to be directly added to phase [8], [12], [13]. Some form of instantaneous AGC is required to justify discarding the amplitude response caused by the same noise, as illustrated in Fig. 3. An additive interference on one side of the carrier frequency [Fig. 3(a)] is mathematically equivalent to the sum of two halves of the same interference plus the difference of two halves of a signal that is the image (equal amplitude, equal offset frequency but on the opposite side of the carrier) of the original interference, as shown in Fig. 3(b). The four halves of sidebands are then regrouped into a pair representing amplitude modulation [Fig. 3(c)], as well as one representing frequency modulation [Fig. 3(d)]. The automatic gain control argument is now invoked to remove the pair representing AM [Fig. 3(e)] and the resulting perturbation is that of the phase

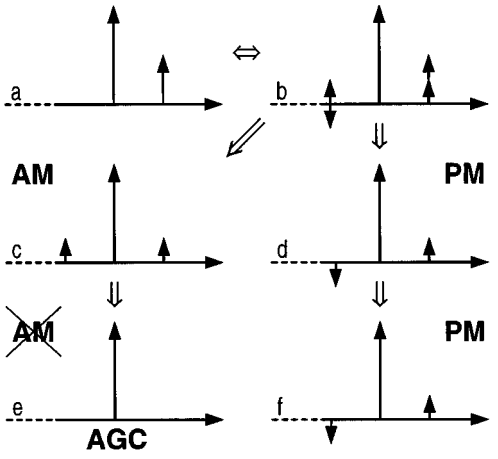

Fig. 3. AGC argument typically used to justify conversion of additive noise to phase noise.

[Fig. 3(f)]. While the AGC argument is an expedient way of modeling an additive interference as phase perturbation, it does not answer the fundamental question if an additive noise always results in only the phase of oscillation being modulated and, when it does, what is the underlying mechanism that causes the conversion of a single-sideband interference into double sidebands with odd symmetry. When AGC is used in an oscillator, it is usually implemented as a narrow-band mechanism to correct slow variations in the steady state oscillation amplitude. Such an AGC only responds to the average noise power, which is constant. There is no reason why one should deliberately construct an instantaneous (wide-band) AGC that is sensitive to added signals often 100 dB below the carrier, especially that we know its only effect would be to turn less harmful additive noise into more harmful phase noise! Indeed, instantaneous or fast-responding AGC's are usually avoided in LC oscillators, precisely to ensure (short-term) frequency stability. Even if one still wanted to construct a wideband AGC, in a high-Q oscillator this would be a very difficult proposition because the time constant of the LC resonator is proportional to the product of Q and the oscillation period and any AGC feedback ultimately must overcome the inertia of the LC resonator to establish a new equilibrium. In very low-Q oscillators (ring oscillators, for instance) inadvertent AGC such as amplitude limiting can be quite fast, but it is inadequate as a fundamental starting point in any general formulation of phase noise theory.

The natural way of modeling the noise input as being additive with the carrier waveform in the time domain has also been adopted in many papers [4], [5], [10]. Some [4], [5] model the nonlinearity of the active device with a third-order term and describe the dynamics of the oscillator with a Van der Pol differential equation driven by the noise source. The resulting analytical expressions, however, have so far predicted a bandpass characteristic. Often a constant term (γ in [4]) is defined which is of the order of magnitude of the relative difference between the small-signal gm of the active device and g_{mc}. This term divided by Q defines the corner of the relative (to the carrier) offset frequency of the pass band of the final output noise, which has not been observed in practical oscillator measurements. Other papers [10] take a general approach of describing arbitrary oscillators with nonlinear state-space equations. While such analyses can be useful for computer aided numerical analysis, the absence of a closed form, explicit solution for any specific oscillator limits their use to a designer to simulation. The dependence of noise of most active devices on the state variables such as instantaneous currents, together with the lack of time-domain description of such a dependence, make it difficult to solve such state-space equations even numerically.

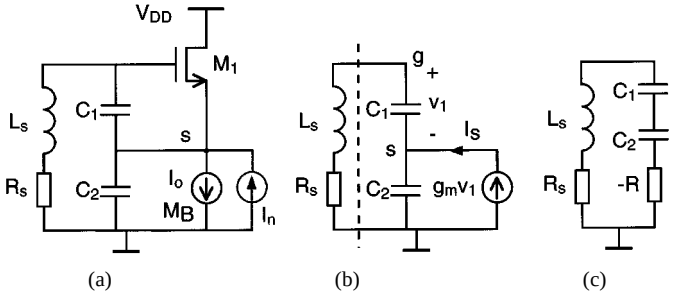

Fig. 4. (a) Minimum representation of a Colpitts oscillator. (b) Equivalent circuit with transistor represented at linear transconductance. (c) Equivalent negative resistance model of oscillator.

The primary purpose of this paper is to provide a formulation of phase noise that is unbiased toward the conclusion, and an analysis that leads to models completely described by direct electrical parameters of an oscillator. In the following, we will first use the CMOS Colpitts oscillator as an example to illustrate an analytical approach to the derivation of both oscillation amplitude and noise response, in Sections II and III respectively. Section IV identifies the noise sources, discusses the dependence of noise source on the varying current in the transistor and derives the noise-to-carrier ratio in the oscillator. Also discussed is the dependence of the N/C ratio on circuit parameters. A brief outline of how the approach to the Colpitts oscillator can be extended to arbitrary LC oscillators will be given in Section V, before the concluding remarks in Section VI.

II. Steady State Amplitude of a CMOS Colpitts Oscillator [31]

We begin with the necessary condition for oscillation for the Colpitts oscillator in Fig. 4(a). For a small carrier signal the MOS transistor can be modeled as a linear gm, as shown in Fig. 4(b). All resistive losses of the tank have been lumped into resistor R_s. The transistor forms a positive feedback loop with capacitors C_1 and C_2. The equivalent impedance Z_R looking to the right of the dashed line in Fig. 4(b) contains a negative real part

$$Z_R = \frac{V}{I} = \frac{1}{j\omega C} + (-R) = \frac{1}{j\omega C_1} + \frac{1}{j\omega C_2} - \frac{g_m}{\omega^2 C_1 C_2}. \quad (1)$$

The necessary condition for the oscillation to start is that the total resistance in the equivalent LC tank in Fig. 4(c) be negative

$$g_m > g_{mc} = \omega_0^2 C_1 C_2 R_s \quad (2)$$

where g_{mc} is defined as the critical transconductance for oscillation and $\omega_0 = 1/\sqrt{(\mathrm{LC})}$ is the tank's angular resonance frequency. A negative middle term in the circuit's characteristic equation means the latter's complex conjugate zeros have a pos-

itive real part. The zero-input response of the circuit is therefore an exponentially increasing sinusoidal oscillation. Equation (2) does not tell us, however, whether the oscillation will stabilize to a particular amplitude.

During startup, the average current in transistor $M1$ may not be the same as the bias current I_o. The difference between the two flows into the capacitive network formed by C_1 and C_2, causing the dc voltage between $M1$'s gate and source V_B to shift. This, in turn, changes the average current in the direction of the bias current. The steady state is reached when the two currents are balanced.

Since the values of the passive components in the tank and their resistive loss, which we will show have a direct impact on oscillation amplitude, have typically 5–20% tolerances an analysis with much greater accuracy is unnecessary for practical purposes. Resonators (tanks) used in oscillators typically have a high quality factor (Q) which suppresses the harmonic contents of any oscillating voltage on the tank to negligible levels. Even for a very low Q of 3–5, typically found in an inductor integrated in a standard CMOS technology, the harmonic content is less than 20%. To restrict the complexity of the analysis we assume that Q is high, so that the harmonics of the tank voltages can be neglected. For the same reason, an elaborate transistor model is also not necessary. Therefore, a simple square-law characteristic is used to describe $M1$

$$I_{DS}(t) = \frac{\beta}{2}[V_{gs}(t) - V_T]^2 \cdot g(t) = \frac{\beta}{2}[V_m \cos(\omega_o t) + V_B - V_T]^2 \cdot g(t) \quad (3)$$

where

- V_m oscillation amplitude;
- V_B dc gate bias in steady state;
- V_T threshold voltage, below which the transistor cuts off and current equals zero.

The gating function $g(t) = 1$ for $V_m \cos(\omega_o t) > (V_T - V_B)$ and $g(t) = 0$ for $V_{gs}(t) \le (V_T - V_B)$. To determine the two unknown variables, steady-state bias ($V_B - V_T$) and oscillation amplitude V_m, we can apply KCL to the s node in Fig. 4(a) at dc and at the resonant frequency to set up two equations.

If the steady-state bias ($V_B - V_T$) is greater than V_m, as depicted in Fig. 5(a), so that $V_m \cos(\omega_o t)$ never causes the transistor to cut off, then the average current through $M1$ is given by

$$I_o = \frac{\omega_o}{\pi}\int_0^{(T/2)} \frac{\beta}{2}[V_m \cos(\omega_o t) + V_B - V_T]^2 dt = \frac{\omega_o \beta V_m^2}{2\pi}\int_0^{(T/2)} [\cos(\omega_o t) - x]^2 dt = \frac{\beta V_m^2}{4}(1 + 2x^2) \quad (4)$$

where x is defined as $(V_T - V_B/V_m)$ and $x \le -1$. The fundamental component of the AC current at ω_o, on the other hand, is given by

$$I_{\omega_o} = \frac{2\omega_o}{\pi}\frac{\beta V_m^2}{2}\int_0^{(T/2)} [\cos(\omega_o t) - x]^2 \cos(\omega_o t) dt = -x\beta V_m^2. \quad (5)$$

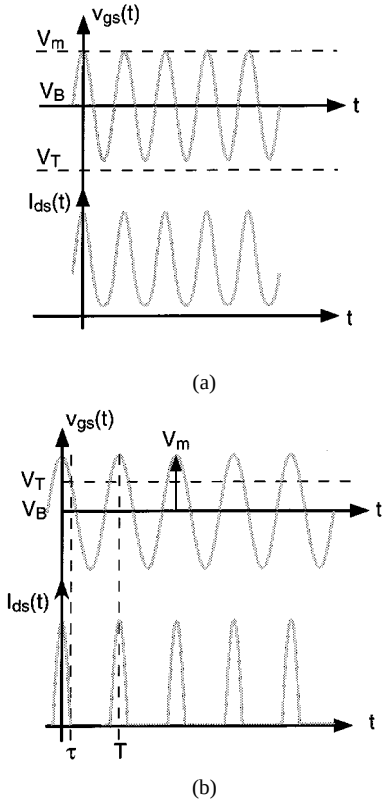

Fig. 5. (a) Voltage and current waveforms when $M1$ is in Class-A mode. (b) Voltage and current waveforms when $M1$ is in Class-C mode.

Multiplying $I_{\omega o}$ with the transimpedance $H(j\omega_o)$ between the I_s branch and V_{gs} branch in Fig. 4(b), we obtain the steady-state oscillation amplitude

$$V_m = I_{\omega_o} H(j\omega_o) = \frac{-x\beta V_m^2}{g_{mc}}. \quad (6)$$

Solving (4) and (6) jointly, we obtain

$$V_m = \frac{\sqrt{2}}{\beta}\sqrt{2\beta I_o - g_{mc}^2}, \text{ and } x = -\frac{g_{mc}}{\beta V_m} \le -1. \quad (7)$$

Reorganizing (7), the same relations can be expressed as

$$\beta V_m = \sqrt{2}\sqrt{2\beta I_o - g_{mc}^2} \le g_{mc}, \quad \text{or } g_{mc}^2 \le g_{mo}^2 = 2\beta I_o \le \tfrac{3}{2} g_{mc}^2. \quad (8)$$

From (7), we see that if one wanted to keep $M1$ from cutting off, a combination of small transconductance coefficient β and large bias current would be the best way to maintain sufficiently large amplitude. The maximum V_m is reached when the second half of (7) is satisfied with equality, in which case $V_{\max} = g_{mc}/\beta$. Condition (8) shows that the range for the nominal transconductance g_{mo} is very small, so that a 20% increase in g_{mc} due to tolerance in capacitance or tank loss can easily kill the oscillation.

To ensure startup as well as adequate amplitude, practical oscillators are designed to have a g_{mo} several times larger than g_{mc}. In this case, conditions in (7) and (8) are no longer satisfied and $M1$ does get cut off during part of the oscillation, as depicted by Fig. 5(b). Equations (4) and (5) must therefore be

modified to account for the time in which $M1$ is cut off. This is done by reducing the limit of integration to the time $M1$ is on

$$\tau = \frac{1}{\omega_o}\cos^{-1}\left(\frac{V_T - V_B}{V_m}\right) = \frac{1}{\omega_o}\cos^{-1}(x), \quad -1 \le x \le 1. \tag{9}$$

The average current through M1 is now given by

$$I_o = \frac{\omega_o \beta V_m^2}{2\pi}\int_0^{(\cos^{-1}(x)/\omega_o)} [\cos(\omega_o t) - x]^2 dt = \frac{\beta V_m^2}{2\pi}\left[\frac{1+2x^2}{2}\cos^{-1}(x) - \frac{3}{2}x\sqrt{1-x^2}\right]. \tag{10}$$

The oscillation amplitude, on the other hand, is given by

$$V_m = I_{\omega_o} H(j\omega_o) = \frac{\omega_o \beta V_m^2}{g_{mc}\pi}\int_0^{(\cos^{-1}(x)/\omega_o)} [\cos(\omega_o t) - x]^2 \cos(\omega_o t) dt = \frac{\beta V_m^2}{3\pi R_s \omega_o^2 C_1 C_2}\left[(2+x^2)\sqrt{1-x^2} - 3x\cos^{-1}(x)\right]. \tag{11}$$

Rearranging (10) and (11), we obtain

$$V_m = \frac{I_o}{g_{mc}} f(x) = \frac{4I_o}{3g_{mc}} \frac{\left[(2+x^2)\sqrt{1-x^2} - 3x\cos^{-1}(x)\right]}{\left[(1+2x^2)\cos^{-1}(x) - 3x\sqrt{1-x^2}\right]} \approx \frac{I_o(5+x)}{3R_s\omega_o^2 C_1 C_2} \tag{12}$$

$$\frac{2\beta I_o}{g_{mc}^2} = \left(\frac{g_{mo}}{g_{mc}}\right)^2 = g^2(x) = \frac{9\pi}{2}\frac{\left[(1+2x^2)\cos^{-1}(x) - 3x\sqrt{1-x^2}\right]}{\left[(2+x^2)\sqrt{1-x^2} - 3x\cos^{-1}(x)\right]^2}. \tag{13}$$

Even without solving (13) explicitly for x, it can be seen from (12) that oscillation amplitude is only a weak function of x and, thus, also of the duty cycle of $M1$. As x varies within its limits ± 1, the amplitude V_m varies by no more than one third. One can thus say that V_m is roughly proportional to the bias current I_o and inversely proportional to g_{mc}. Fig. 6 compares the exact function $f(x)$ and its approximation $(5+x)/3$ in (12). The maximum difference is less than 2%, occurring at $x = 0$, which is a negligible error in terms of amplitude prediction. The approximate version of (12) has the advantage of much greater simplicity.

Although a solution for x in explicit form is more difficult to obtain from (13), it is only a function of $M1$'s nominal transconductance g_{mo} normalized to the g_{mc} of the passive tank. Thus, x needs to be solved only once numerically versus a useful range of normalized g_{mo} and can be looked up once the ratio between g_{mo} and g_{mc} is known. Fig. 7 shows the calculated x and the

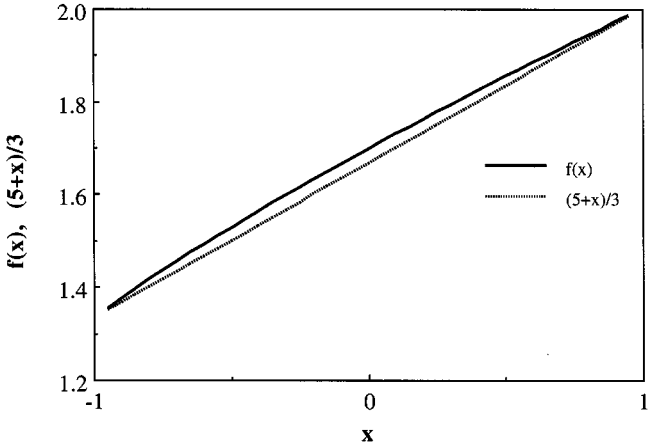

Fig. 6. Comparison of $f(x)$ with its approximation

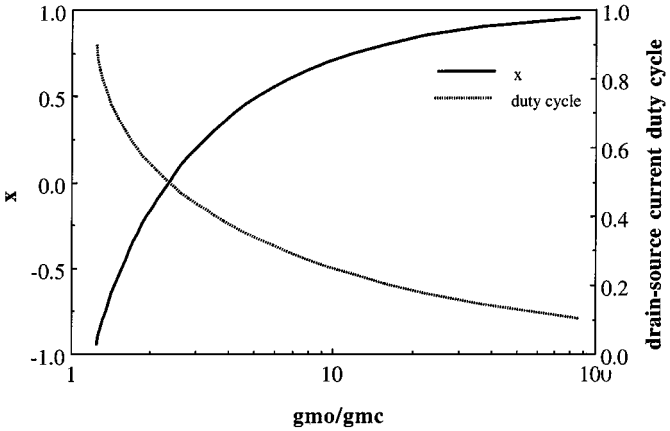

Fig. 7. Parameter x and duty cycle as a function of normalized nominal gm of $M1$.

corresponding duty cycle $\alpha = 2\tau/T = \cos^{-1}(x)/\pi$ versus (g_{mo}/g_{mc}). Note that the horizontal axis is on logarithmic scale to allow the low-g_{mo}/g_{mc} region to be better displayed. It can be seen that both $x$and the duty cycle are relatively steep functions when the normalized g_{mo} of $M1$ is low. For a g_{mo}/g_{mc} ratio of three, which can be easily expected for practical designs $x = 0.2$ and $\alpha = 44\%$. The improvements of x and α are much slower beyond $g_{mo}/g_{mc} > 5$, resulting only in $0.5 < x < 1$ and $\alpha < 33\%$ so that setting $M1$'s transconductance much higher than the g_{mc} of the tank is inefficient as far as achieving better amplitude is concerned. The limit in V_m is achieved when g_{mo}/g_{mc} tends to infinity, in which case x tends to unity and

$$V_m = \frac{2I_o}{g_{mc}}. \tag{14}$$

It is interesting to note that this limit is independent of the detailed parameters of $M1$. In fact, the limit is exactly the same if $M1$ in Fig. 4(a) is replaced by a bipolar transistor [30]. It is also worth noting that the duty cycle of $M1$ is 0% in the limit and only 33% for $g_{mo}/g_{mc} = 5$. This indicates that the active device, be it MOS or BJT, operates deeply in class-C mode in a typical LC oscillator. In other words, the active device behaves more like a switch than an amplifier. To demonstrate this, we replace the active transistor in the Colpitts oscillator by a switch, in series with a current source I_{pulse}, as shown in Fig. 8(a). The

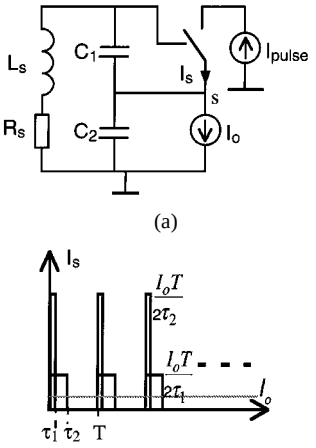

Fig. 8. Thought experiment. (a) Colpitts oscillator with ideal switch (b) Current versus duty cycle

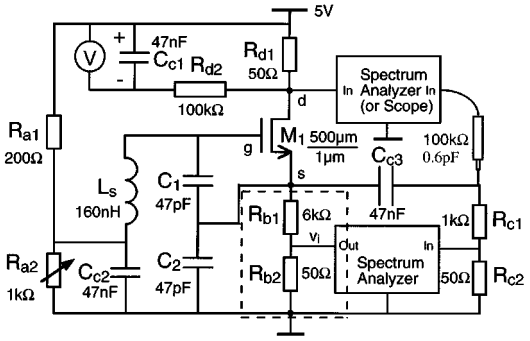

Fig. 9. Colpitts oscillator constructed for measuring amplitude and duty cycle, as well as the responses to injected sinusoidal current

threshold of the switch is set relative to the s node of the circuit. If $I_{\rm pulse}$ is larger than I_o, the dc voltage across capacitor C_1 will change relative to the threshold of the switch so as to restrict the period the switch is turned on. The constraint is that the average current through the switch equals the bias current, $I_{\rm pulse} \bullet 2\tau/T = l_o$. If we increase the available current $I_{\rm pulse}$ further and further, the duty cycle of the switch becomes smaller and smaller, as depicted by Fig. 8(b) [29], [32], until the current through the switch becomes a Dirac function of area l_oT. Thus, irrespective of how the switch is constructed, as long as a large current is available during its on period, the limit of the oscillation amplitude is

$$V_m = \left(\frac{1}{g_{mc}}\right)\frac{2}{T}\int_0^T I_oT\delta(t)e^{-j\omega_o t}\,dt = \frac{2I_o}{g_{mc}}. \qquad (15)$$

The examples of BJT and MOS implementations show that the details of the switch construction determine how fast the limit in (15) is reached. As long as the active device, be it BJT, MOS, or any other switch-like transistor, has sufficient transconductance, the details are unimportant as the amplitude will be close to the limit set by (15). In practical designs, insight into the approximate amplitude dependence on the circuit parameters can be obtained from (15), whereas a more precise estimate can be obtained from (12).

To verify (12), SPICE simulations as well as experiments have been performed. The simulated amplitude agrees with (12) to within 1% for $Q > 50$. For a moderate Q of around 10, the simulated amplitude is about 1–2 dB below that predicted by (12). To perform controlled experiments, a 78-MHz Colpitts oscillator is constructed, as shown in Fig. 9, where the values of the main oscillator, as well as those of biasing and coupling components, can be found. The choice of the oscillation frequency was made to be sufficiently low to allow values of the resonator inductor and capacitors to be much higher than board-level parasitics and yet sufficiently high so that the conclusions from the measurements remain valid for high frequency oscillators at the low-gigahertz range.

The transistor $M1$ has a transconductance coefficient of 90 μA/V^2 and was produced in a 1-μm CMOS process. Before mounting the transistor, the equivalent parallel resistance R_p of the tank at resonance has been measured and the value of the parallel resistance R_{c1} is selected accordingly, to make the resulting R_p exactly 500 Ω (or $g_{mc} = 2$ mS) at resonance. The gate bias voltage is adjusted by means of R_{a2} to ensure that the measured dc current through $M1$ is 0.5 mA during steady-state oscillation. The corresponding $g_{mo} = 6.7$ mS. According to Fig. 7, $x = 0.275$ and the duty cycle $\alpha = 0.41$, whereas the oscillation amplitude is 0.44 V according to (12). Fig. 10 shows the measured steady-state source and drain voltages of $M1$. The oscillation amplitude at the source is 450 mV, whereas the duty cycle, measured as the time between the two cursor positions of the drain voltage waveform divided by the oscillation period, is 0.414. Further measurements of a similar oscillator for four different g_{mc}'s versus bias current from 200 μA to 5 mA [31] show that the amplitude prediction by (12) is always within 1 dB of measured values. Since normal tolerances of both the resonance and the loss of LC tanks, whether made of SMD components or integrated on silicon, can be easily 5%–20%, the tolerance in g_{mc} can be easily a couple of decibels. The accuracy of (12) is therefore as good as need be for practical design purposes.

III. Oscillator Response to an Interfering Current

To analyze the oscillator response to interference, let us inject a small current [shown in gray in Fig. 4(a)], $I_n \cos[(\omega_0 + \Delta\omega)t + \phi_n]$, into the s node. Although the phase of the injected current is not important, we assume it is ϕ_n for the sake of generality, while the main oscillation (carrier) serves as the reference, so that its phase is assumed zero. Any response at $\omega_0 + \Delta\omega$ by $M1$'s gate-source voltage will be modulated by the gating function $g'(t)$, which is nearly the same as $g(t)$.

$$g'(t) \approx g(t) = \left[\frac{2\tau}{T} + \sum_{i=1}^{\infty}\frac{2\sin(i\omega_o\tau)}{i\pi}\cos(i\omega_o t)\right] \left(0 < \alpha = \frac{2\tau}{T} < 100\%, \rightarrow |x| < 1\right). \qquad (16)$$

Due to this modulation, a response voltage will also be created at the image frequency $\omega_0 - \Delta\omega$, which itself will be modulated to create a feedback component at $\omega_0 + \Delta\omega$. At this stage, we only know that there will be a voltage response at both $\omega_0 + \Delta\omega$ and $\omega_0 - \Delta\omega$, but their amplitude and phase in steady-state V_u, ϕ_u

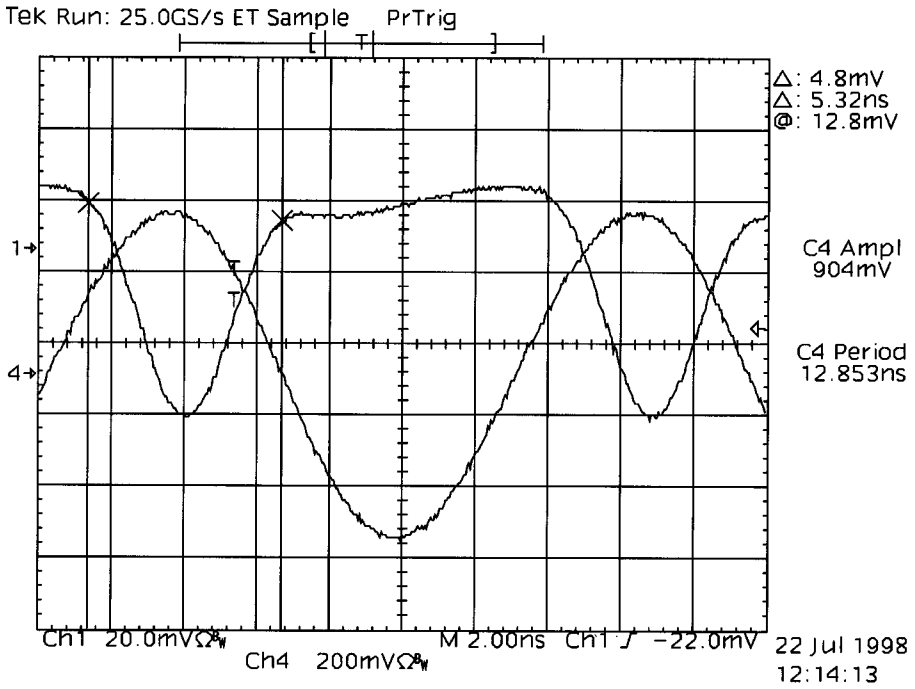

Fig. 10. Measured oscillation waveforms. Channel 1: $M1$'s drain voltage representing its drain current. Channel 4: $M1$'s source voltage

and V_L, ϕ_L for the upper and lower sidebands, respectively, are unknown to us.

$$\begin{aligned} V_{gs}(t) &= V_B + V_m\cos(\omega_o t) + \Delta v \\ &= V_B + V_m\cos(\omega_o t) + V_u\cos[(\omega_o+\Delta\omega)t+\phi_u] \\ &\quad + V_L\cos[(\omega_o-\Delta\omega)t+\phi_L]. \end{aligned} \tag{17}$$

The perturbed feedback current through $M1$ is therefore approximately given by

$$\begin{aligned} I_{DS}(t) \approx \frac{\beta}{2}&\{V_m\cos(\omega_o t) + V_B - V_T \\ &+ V_u\cos[(\omega_o+\Delta\omega)t+\phi_u] \\ &+ V_L\cos[(\omega_o-\Delta\omega)t+\phi_L]\}^2 \\ &\cdot\left[\frac{2\tau}{T} + \sum_{i=1}^{\infty}\frac{2\sin(i\omega_o\tau)}{i\pi}\cos(i\omega_o t)\right]. \end{aligned} \tag{18}$$

Expanding (18), we collect only the terms at the interference frequency $\omega_o+\Delta\omega$ and the image $\omega_o-\Delta\omega$, because they will be fed back to the gate of the tank to sustain the interfering voltages. The terms around dc and higher harmonics of ω_o can be neglected, because they will be heavily attenuated by the (high-Q) tank and will not produce much voltage on the gate. Since the current and voltage perturbations are assumed much smaller than the main carrier, their second- and higher order combinations are negligible. Thus, the significant part of $\Delta I_{DS}(t)$, $\Delta I'_{DS}(t)$, is given by

$$\begin{aligned} \Delta I'_{DS}(t) = &\frac{\beta V_m}{3\pi}\left[(2+x^2)\sqrt{1-x^2} - 3x\cdot\cos^{-1}(x)\right] \\ &\cdot\{V_u\cos[(\omega_o+\Delta\omega)t+\phi_u] \\ &\quad + V_L\cos[(\omega_o-\Delta\omega)t+\phi_L]\} \\ &+ \frac{\beta V_m}{3\pi}(1-x^2)^{3/2} \\ &\cdot\{V_u\cos[(\omega_o+\Delta\omega)t+\phi_u] \\ &\quad + V_L\cos[(\omega_o-\Delta\omega)t+\phi_L] \\ &\quad + V_L\cos[(\omega_o+\Delta\omega)t-\phi_L] \\ &\quad + V_u\cos[(\omega_o-\Delta\omega)t-\phi_u]\}. \end{aligned} \tag{19}$$

It is interesting to note that the coefficient of the first term on the right-hand side of (19) is the same as g_{mc}, the amount of gm required to cancel the loss of the resonator, according to (11). Typically, $|x|\neq 1$, so that an apparent excess term exists in the gm between the upper sideband (USB) voltage perturbation on the gate and the current perturbation in $M1$, unless the USB and LSB (lower sideband) responses are equal in amplitude and opposite (180°) in phase, such that the second term in (19) is always cancelled.

The four unknown parameters of the voltage perturbation around the fundamental frequency can be related to the injected current by Kirchhoff's current law on the s node in Fig. 4(a)

$$I_{\omega o}\cos(\omega_o t) + \Delta I'_{DS}(t) + I_n(t) + C_1\frac{dV_1}{dt} - C_2\frac{dV_2}{dt} = 0. \tag{20}$$

It can be shown that for $\Delta\omega \ll \omega_o$

$$\begin{aligned} C_1\frac{dV_1}{dt} - C_2\frac{dV_2}{dt} \approx &2(C_1+C_2)\Delta\omega \\ &\cdot\{V_u\sin[(\omega_o+\Delta\omega)t+\phi_u] \\ &\quad - V_L\sin[(\omega_o-\Delta\omega)t+\phi_L]\} \\ &- R_s C_1 C_2\omega_o^2 \\ &\cdot\{V_m\cos(\omega_o t) \\ &\quad + V_u\cos[(\omega_o+\Delta\omega)t+\phi_u] \\ &\quad + V_L\cos[(\omega_o-\Delta\omega)t+\phi_L]\}. \end{aligned} \tag{21}$$

Combining . (11), (19) and (21) into (20), we obtain

$$\begin{aligned}&\frac{\beta V_m}{3\pi}(1-x^2)^{3/2}\\&\quad\cdot\{V_u\cos[(\omega_o+\Delta\omega)t+\phi_u]\\&\qquad+V_L\cos[(\omega_o-\Delta\omega)t+\phi_L]\\&\qquad+V_L\cos[(\omega_o+\Delta\omega)t-\phi_L]\\&\qquad+V_u\cos[(\omega_o-\Delta\omega)t-\phi_u]\}+2(C_1+C_2)\Delta\omega\\&\quad\cdot\{V_u\sin[(\omega_o+\Delta\omega)t+\phi_u]\\&\qquad-V_L\sin[(\omega_o-\Delta\omega)t+\phi_L]\}\\&\quad+I_n\cos[(\omega_o+\Delta\omega)t+\phi_n]\\&=A\cdot\cos[(\omega_o+\Delta\omega)t]+B\cdot\sin[(\omega_o+\Delta\omega)t]\\&\quad+C\cdot\cos[(\omega_o-\Delta\omega)t]+D\cdot\sin[(\omega_o-\Delta\omega)t]=0.\end{aligned}\tag{22}$$

For (22) to be valid at all times, the coefficients for the sine and cosine terms at both frequencies must be zero. This provides us with four simultaneous equations to solve for the four unknowns in steady state V_u, ϕ_u, V_L and ϕ_L

$$\begin{aligned}A=&\frac{\beta V_m}{3\pi}(1-x^2)^{3/2}[V_L\cos(\phi_L)+V_u\cos(\phi_u)]\\&+2(C_1+C_2)\Delta\omega V_u\sin(\phi_u)+I_n\cos(\phi_n)=0\end{aligned}\tag{23}$$

$$\begin{aligned}B=&\frac{\beta V_m}{3\pi}(1-x^2)^{3/2}[V_L\sin(\phi_L)-V_u\sin(\phi_u)]\\&+2(C_1+C_2)\Delta\omega V_u\cos(\phi_u)-I_n\sin(\phi_n)=0\end{aligned}\tag{24}$$

$$\begin{aligned}C=&\frac{\beta V_m}{3\pi}(1-x^2)^{3/2}[V_L\cos(\phi_L)+V_u\cos(\phi_u)]\\&-2(C_1+C_2)\Delta\omega V_L\sin(\phi_L)=0\end{aligned}\tag{25}$$

$$\begin{aligned}D=&\frac{\beta V_m}{3\pi}(1-x^2)^{3/2}[V_u\sin(\phi_u)-V_L\sin(\phi_L)]\\&-2(C_1+C_2)\Delta\omega V_L\cos(\phi_L)=0.\end{aligned}\tag{26}$$

If we redefine the four knowns as $V_u^R=V_u\cos(\phi_u)$, $V_u^I=V_u\sin(\phi_u)$, $V_L^R=V_L\cos(\phi_L)$ and $V_L^I=V_L\sin(\phi_L)$, it is quite clear that (23)–(26) are linear and readily solvable. Solving (23)–(26) jointly and defining ϕ_c in (27), we find

$$\phi_c=\tan^{-1}\left[\frac{6\pi(C_1+C_2)\Delta\omega}{\beta V_m(1-x^2)^{1.5}}\right]\tag{27}$$

$$\begin{aligned}\phi_L=&\tan^{-1}\left[\frac{\beta V_m(1-x^2)^{1.5}}{3\pi(C_1+C_2)\Delta\omega}\right]-\phi_n+k\pi,\\&k=0,\,1,\,2\cdots\end{aligned}\tag{28}$$

$$\phi_u=\pi-\phi_L-\phi_c\tag{29}$$

$$V_L=V_u\cos(\phi_c)\tag{30}$$

$$\begin{aligned}V_u^2=&\frac{I_n^2}{[2(C_1+C_2)\Delta\omega]^2[1+3\cdot\cos^2(\phi_c)]}\\=&\frac{I_n^2}{[2(C_1+C_2)\Delta\omega]^2}\\&\cdot\frac{[\beta V_m]^2(1-x^2)^3+[6\pi(C_1+C_2)\Delta\omega]^2}{\{4\cdot[\beta V_m]^2(1-x^2)^3+[6\pi(C_1+C_2)\Delta\omega]^2\}}.\end{aligned}\tag{31}$$

Usually the offset frequency is relatively small, $6\pi(C_1+C_2)\Delta\omega\ll\beta V_m(1-x^2)^{3/2}$, so that $\phi_c\approx 0$, $V_u=V_L$, and $\phi_u\approx\pi-\phi_L$. The upper and lower sideband responses are therefore equal in amplitude and 180° out of phase. This is just the same as what would be created by a modulation in phase, so that additive interference does create phase modulation, due to the switching behavior of $M1$. For the same low-offset frequencies

$$V_u^2\approx\frac{I_n^2}{4\cdot[2(C_1+C_2)\Delta\omega]^2}\text{ or }V_u\approx\frac{I_n}{4\cdot(C_1+C_2)\Delta\omega}.\tag{32}$$

Note that (32) is half of what would be predicted by a linear analysis. The USB response is indeed inversely proportional to the offset frequency, as has been well known experimentally. This inverse dependence does not continue uninterrupted, however, according to (31). At sufficiently high-offset frequencies $6\pi(C_1+C_2)\Delta\omega\gg 2\beta V_m(1-x^2)^{3/2}$ and the transistor no longer has sufficient gm to provide any significant feedback to counter the interfering current so that the relationship between the latter and the voltage response is purely that of a linear tank. The image sideband then disappears, according to (27) and (30). The result is now identical to that predicted by a linear analysis

$$V_u\approx\frac{I_n}{2\cdot(C_1+C_2)\Delta\omega}.\tag{33}$$

The transition point where the image sideband response V_L becomes 3 dB below the upper sideband response V_u can also be derived from (30)

$$\Delta\omega_{-3\text{ dB}}=\frac{\beta V_m(1-x^2)^{1.5}}{6\pi(C_1+C_2)}.\tag{34}$$

For oscillators with 100% current duty cycle $x\le -1$, the corner frequency is zero and the noise remains additive because there is no more gating function and the squaring nonlinearity of the MOSFET only translates the upper sideband interfering signal to frequencies around DC and the second harmonic of the carrier, which will be suppressed by the carrier. When x tends to 1, as in the case of a lossless resonator, the corner frequency also tends to zero and the output noise remains additive. For most practical oscillators $|x|<1$ and noise becomes multiplicative, affecting the phase of oscillation. The −3-dB offset frequency given in (34) is usually too high to be observed in normal phase noise measurements because the sideband spectral density at such a frequency is already well below the noise floor of the measuring instruments.

It is important to note from (32)–(34) that the detailed transistor parameters are only important in determining the boundary between the interferences that will merely be superimposed on the main oscillation and those that will cause jitter in the phase of the oscillation. In the former case, the $1/\Delta\omega$ characteristic is merely due to the impedance of the linear tank decreasing. In the latter case, the creation of the image response and the effective negative feedback loop (through modulation) between the signals at the two frequencies are responsible for canceling any excess gm of $M1$ that is not needed for compensating the loss of the passive tank. Although in both cases the response is inversely proportional to offset frequency, the two cases differ by 6 dB and cause very different

disturbances to the oscillator. In the phase jitter case both the image response and its interaction with the response at the frequency of interference are due to the active device's nonlinearity, especially the switching action in most oscillators. Analyses attempting to bypass the explicit description of the transistor's nonlinearity therefore bypass the most fundamental mechanism in amplitude to phase noise conversion. The mixing action (by switching) alone creates the image sideband, which does not necessarily entail the odd symmetry of phase modulation. The fact that the image signal is mixed back to the original sideband in an oscillator, however, means a feedback loop between the signals at the two frequencies is created by mixing. In a stable oscillator, this feedback must be negative unless the loop gain is (much) less than unity as in the case of a high-offset frequency. A strong negative feedback is only feasible if the image response is delayed in the transient, such that its steady-state phase is 180° offset from the response at the original frequency. This creation of negative feedback in the transient by relative phase shift is somewhat analogous to the locking process in a phase locked loop [33]. Balance of currents at the image frequency [(25), (26)], where there is no input, then forces the two steady-state sideband responses to have equal amplitude and the effective gain of the negative feedback loop to be unity. The close-loop (low-offset) response at the original frequency is therefore half of the open-loop (high-offset) response, as described by (32) and (33).

The exact amount of $M1$'s gm, and indeed the detailed shape of its large-signal *V–I* characteristic, are otherwise unimportant except in setting the boundary between conversion and no conversion to phase noise.

The significance of the theoretical prediction of the crossover point and indeed its experimental verification lies therefore not so much in the 6-dB difference in noise prediction at higher frequencies as in being a litmus test of the rigorousness of the formulation of a noise analysis. The crossover point is usually so far away in relative offset frequency from the carrier that the noise there and beyond is too low to affect any practical design. The fact that its existence has never been noted before is ample proof. This existence enables us to make two observations that are both fundamental and common sensical: 1) interfering noise close to the carrier causes phase modulation that results in a double-sideband odd-symmetric response and 2) interference far away from the oscillation frequency causes no more than additive noise. In the latter case, the response must be very similar to that of a passive tank alone. In recent literature on phase noise [12], [34], it has been forcefully argued that some time variant nature of the oscillator's impulse response, rather than the nonlinearity of the active device, plays the fundamental role in the creation of phase noise or DSB response to an SSB interference. So much so that only a lossless LC tank with an additive current source has been used as the basis for the formulation of subsequent analyses and no distinction is made between low and high-offset frequencies in the formulation of the theory and its conclusions. It is perhaps worth pointing out that a lossless LC tank, being a linear network, is incapable of generating a second sideband, let alone the odd symmetry between the two sidebands. For a lossy oscillator and finite transconductance of any transistor, the voltage response at high-offset frequencies

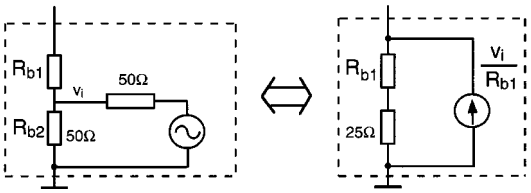

Fig. 11. The Norton equivalent representation of the subcircuit devised to inject controlled current into the oscillator

eventually becomes too low to allow the transistor to feed back significant current to counter the injected interference. The response must therefore be that of a linear network and no image sideband should be observed. In our analysis, the results reduce to that of a lossless tank naturally if we let the loss resistance R_s and bias current I_o tend to zero simultaneously under the constraint of a constant oscillation amplitude. The current duty cycle in the transistor then tends to zero ($x \rightarrow 1$), which means the latter is permanently cut off and does not affect the oscillation. The crossover frequency in (34) also tends to zero, which means that the response is given by (33), that of a linear network, without any image.

To verify the results in this section, the oscillator in Fig. 9 is used to test its voltage response to an injected deterministic current. Since the equivalent input impedance at the s node can be very high at close to the resonance frequency of the tank, injecting a well-known current is difficult. Instead of applying a current directly, we apply a sinusoidal voltage, as shown, and measure the voltages V_s and V_i. The Norton equivalent of the circuit within the dashed box in Fig. 9 is shown in Fig. 11. Since the effective injected current is given by V_i/R_{b1}, the impedance Z looking into the s node of the oscillator from the equivalent current source is the measured node voltage V_s divided by V_i/R_{b1}, $Z = (V_s/V_i)R_{b1}$. Since for a low-loss tank the current flowing through C_1 and C_2 at close to resonance is much higher than other current components flowing into the s-node, the latter can be neglected and $V_{gs}(t) = (C_1/C_2)V_s(t)$. The transimpedance $Z_T = V_{gs}/I_n$ can therefore be reliably measured, at least in the vicinity of the carrier, via the voltage ratio (V_s/V_i). Close to the carrier, the applied signal levels are kept very small to avoid pulling the main oscillation. As $\Delta\omega$ is gradually increased, the voltage response becomes so small that it sinks below the noise floor of the spectrum analyzer. The interfering signal level is increased when necessary just to keep the spectral peaks representing the voltage response above the noise floor by a few decibels. Also measured are the ratio between the voltage response at the image frequency and the injected current, which we refer to as the image transimpedance.

The measured transimpedances are shown in Fig. 12, against those calculated using (30) and (31). Also shown is the straight line to which the upper sideband transimpedance is asymptotic at higher offset frequencies, which would result from a linear analysis. The measurements and calculations agree to within 1 dB at low-offset frequencies and 2 dB at high-offset frequencies, which is remarkable over nearly six decades of offset frequency and seven decades of impedance levels. Also remarkable is the accurate prediction of the crossover point at 1.3 MHz. This shows that as long as the parasitics are small and the oscillator

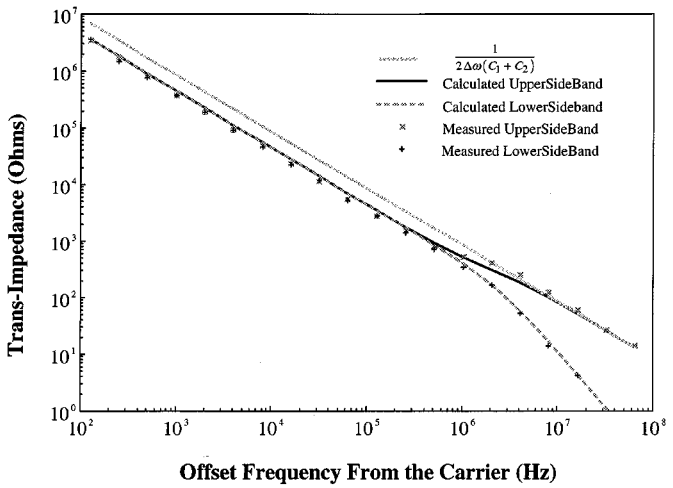

Fig. 12. Calculated and measured voltage responses at both the upper sides and and lower sideband to injected current at upper sideband (the circuit parameters are slightly different from those in Fig. 10: $V_m = 0.37$ V and $x = 0.2$).

can be truly represented by Fig. 4(a), then the formulas derived above are very accurate.

A further point to note from Fig. 12 is that the $1/\Delta\omega$ characteristic continues all the way down to 100-Hz offset, where further measurement was prevented by the drift of the free-running oscillator. An early measurement of a Clapp oscillator at a similar carrier frequency, locked to a crystal oscillator by a very narrow-band PLL to reduce drift, showed that such a $1/\Delta\omega$ characteristic continues to nearly 10 Hz. The experiments therefore demonstrate that analyses predicting a much higher corner frequency are incorrect. Below such offsets, pulling must be dominant so that the exact shape of phase noise should be immaterial. At the high-offset end, our measurements show that the $1/\Delta\omega$ characteristic continues until 64 MHz, further than two thirds of the carrier frequency itself! No flattening is observed, so that part of Leeson's description of the phase noise spectrum is incorrect. The experimental results are to be expected although, because it would be very hard to imagine what noise mechanism would create a response of constant amplitude on a passive tank while the latter's impedance gradually declines to zero! The flat noise spectrum we sometimes do see in practical oscillators must have come from buffers rather than the LC oscillator proper.

The analysis of the oscillator response to a single sinusoidal interfering current at a single offset frequency can easily be extended to multiple signals at different offset frequencies. If the sum of all the interfering signals is small compared to the carrier, then one can assume that the interfering current at each offset frequency will generate a pair of response voltages. As long as we can neglect the second- and higher order combinations of interfering voltage components in the Taylor expansion of the feedback currents, the subsequent mathematical manipulations can be considered linear because multiplication by $g(t)$ only results in frequency translation of each component. Thus, each pair of voltage responses can be solved at the corresponding offset frequency and its image. In this sense, the oscillator response to the composite current of different frequencies is the superposition of the responses to the current components at each frequency. This enables our noise analysis to follow all the reasoning of noise analyses of common linear networks.

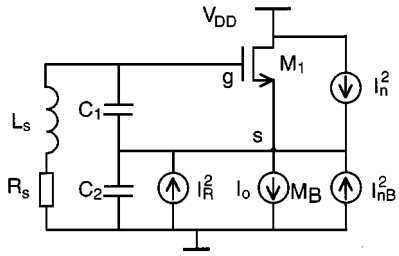

Fig. 13. Colpitts oscillator with all noise sources represented as current into the S node.

IV. Noise to Carrier Ratio in a CMOS Colpitts Oscillator

If the offset frequency is much higher than $\Delta\omega_{-3\text{ dB}}$ [(34)], the noise spectral density of the oscillator gate-source voltage at each frequency is simply given by (33) times the spectral density of equivalent noise current at that frequency. In the much more important case that the offset frequency is below $\Delta\omega_{-3\text{ dB}}$, the response is given by (32) times the spectral density of equivalent noise current at the same frequency plus the contribution due to the image of noise current component at the other side of the carrier

$$V_n^2(\omega_o+\Delta\omega) = \frac{I_n^2(\omega_o+\Delta\omega)}{16\cdot(C_1+C_2)^2\Delta\omega^2} + \frac{I_n^2(\omega_o-\Delta\omega)}{16\cdot(C_1+C_2)^2\Delta\omega^2} + C'\frac{I_n(\omega_o+\Delta\omega)I_n^*(\omega_o-\Delta\omega)}{8\cdot(C_1+C_2)^2\Delta\omega^2}. \quad (35)$$

In (35) C' represents the cross-correlation factor between the two noise components. For white noise it is reasonable to assume that noise components at different frequencies are uncorrelated to each other, $C' = 0$, so that the noise voltage spectral density is given by

$$V_n^2(\omega_o+\Delta\omega) = \frac{I_n^2}{8\cdot(C_1+C_2)^2\Delta\omega^2}. \quad (36)$$

Experiments will be compared to (36) later to verify the assumption $C' = O$.

Now that we have established the relationship between phase noise spectrum and the input white noise current, what remains to be done is to identify all major noise sources in the Colpitts oscillator. In the order of increasing importance, they are the noise current associated with the bias transistor MB, noise current due to the loss resistance R_s of the tank, and the noise current due to the main switching transistor $M1$. If we can convert all three sources into equivalent current sources, as shown in Fig. 13, then the total output noise can be easily obtained by applying (36).

Since the drain of MB is directly connected to the s node and its current is constant, the noise current due to MB is the most straightforward, $I_{nB}^2 = \gamma 4KTg_{\text{MB}}$, where $\gamma = 2/3$ for long channel devices. The noise contribution of R_s can be worked out

via the Norton equivalent current at the s node. Representing the noise of R_s as a voltage source and short-circuiting the s node, we can obtain the mean-squared current noise power spectral density (psd) of the Norton equivalent circuit near the resonant frequency, $I_R^2 \approx (\omega C_2)^2 \cdot 4kTR_s = (C_2/C_1) \cdot 4kT \cdot g_{mc}$.

The time-varying nature of its drain-source current makes $M1$ a more complex noise source. Referring to Fig. 8(b), the average current through $M1$ during the time it is on is given by (37). The average white noise

$$I'_{m1} = \frac{I_o}{\alpha} = I_o \left(\frac{T}{2\tau}\right) = I_o \frac{\pi}{\cos^{-1}(x)} \tag{37}$$

$$\begin{aligned} I^2_{n'} &= \gamma 4kT g'_{m1} \\ &= \gamma 4kT \sqrt{2\beta I_o \frac{\pi}{\cos^{-1}(x)}} \\ &= \gamma 4kT g_{mo} \sqrt{\frac{\pi}{\cos^{-1}(x)}} \end{aligned} \tag{38}$$

psd during $M1$'s on time is therefore given by (38). If a time-domain signal $n'(t)$ has the same psd as that given by (38), then the noise current for $M1$ is equivalent to $n'(t)$ gated by $g(t)$. Since $n'(t)$ has a bandwidth much wider than the frequency of the gating function, the psd of $n(t)$ around the oscillation frequency is that of $n'(t)$ scaled by the duty cycle of $g(t)$ [35], $\alpha = \cos^{-1}(x)/\pi$.

$$I_n^2 \approx \frac{\cos^{-1}(x)}{\pi} I^2_{n'} = \gamma 4kT g_{mo} \sqrt{\frac{\cos^{-1}(x)}{\pi}}. \tag{39}$$

A more accurate estimate of I_n^2 is possible by splitting $M1$'s on time into infinitely small intervals, each one $d\tau$ wide, to allow the exact current to be used for each interval instead of the average in (38). Since the noise contribution of each $d\tau$ interval can be calculated with a gating duty cycle of $d\tau/T$, the overall noise psd is the sum of the individual contributions, which amounts to an integration that leads to

$$I_n^2 = \gamma 4kT\beta V_m \frac{\sqrt{1-x^2} - x\ \cos^{-1}(x)}{\pi}. \tag{40}$$

Since most practical oscillators already have fairly low duty cycles, the difference between (39) and (40) is fairly small. [For the circuit in Fig. 9 the overall noise estimate using (40) is about 0.5 dB below that using (40)]. Equation (39) is therefore more preferable because it gives one more insight into the relationship between noise and the nominal transconductance, as well as the current duty cycle. The latter two are design parameters.

Replacing the noise current term in (36) with the sum of contributions from the bias transistor, the resistive loss of the tank and that of the switching transistor $M1$, we obtain

$$\begin{aligned} V_n^2(\omega_o + \Delta\omega) &= V_n^2(\omega_o - \Delta\omega) \\ &= \frac{kT}{2 \cdot (C_1 + C_2)^2 \Delta\omega^2} \\ &\quad \cdot \left[\gamma g_{mB} + \left(\frac{C_2}{C_1}\right) g_{mc} + \gamma g_{mo} \sqrt{\frac{\cos^{-1}(x)}{\pi}}\right]. \end{aligned} \tag{41}$$

The ratio between the noise psd and the signal power can now be derived by combining (12) and (41)

$$\begin{aligned} S^{\Delta\omega}_{N/C} &= \frac{2 \cdot V_n^2(\omega_o + \Delta\omega)}{V_m^2} = \left(\frac{3}{5+x}\right)^2 \frac{kT}{I_o^2 Q^2} \left(\frac{\omega_o}{\Delta\omega}\right)^2 \\ &\quad \cdot \left[\gamma g_{mB} + \left(\frac{C_2}{C_1}\right) g_{mc} + \gamma g_{mo} \sqrt{\frac{\cos^{-1}(x)}{\pi}}\right]. \end{aligned} \tag{42}$$

For small duty cycles x is close to 1, (42) is then approximately given by

$$\begin{aligned} S^{\Delta\omega}_{N/C} &\approx \frac{kT}{I_o^2 Q^2} \left(\frac{\omega_o}{2\Delta\omega}\right)^2 \\ &\quad \cdot \left[\gamma g_{mB} + \left(\frac{C_2}{C_1}\right) g_{mc} + \gamma g_{mo} \sqrt{\frac{\cos^{-1}(x)}{\pi}}\right]. \end{aligned} \tag{43}$$

To verify (42), the parameters in Fig. 9 were used to calculate the oscillator output spectral density due to thermal noise sources. The noise contributions in the square brackets in (42) are 0.17 mS for the 6-kΩ bias resistor, 2 mS for the rest of the resistive loss of the passive tank that had been measured before $M1$ was mounted, and 2.86 mS due to $M1$. The quality factor Q of the tank is slightly under 25. This yields a calculated phase noise of $-$ 115 dBc/Hz at 10-kHz offset. The calculated phase noise is compared with measured results in Fig. 14, covering four octaves of offset frequency range. Because the oscillator was designed to be relatively high Q, the overall phase noise is very low. The noise floor of the instrument and the onset of up-converted flicker noise therefore limit the measurable thermal noise region to the last two octaves. This gives us three measurement points that are clearly on the 6 dB/oct line. To remove the influence of the noise from the instrument (HP 8563E Spectrum Analyzer), the latter is calibrated by measuring an 80-MHz crystal oscillator at the corresponding offset frequencies. Since the phase noise of an 80-MHz crystal oscillator is better than $-$110 dB at 300-Hz offset [36], the measured noise at offsets above 1 kHz is effectively that of the instrument. This uncorrelated noise contribution of the instrument is then subtracted from the measured noise power at the 10-kHz and 20-kHz offset points. As is typical of most noise measurements, the repeatability of the measured noise power spectral density (with averaging) is approximtely within 0.5–1 dB. The measurement accuracy of the points shown in Fig. 14 can therefore be considered to be 1 dB. This is the same accuracy with which the calculated thermal noise line in Fig. 14 predicts the measurement. The measurement at 1.25 kHz is 16 dB higher than that at 5 kHz, showing this region to be strongly influenced by flicker noise. From the slope of the measured noise psd we can infer that the crossover point between thermal noise and flicker noise is around 1.5 kHz. Adding the inferred flicker noise to the calculated white noise contribution, we have a calculated phase noise that also agrees with measurement within 1 dB for the first two octaves of measured offset frequency. This can be seen as conclusive evidence that (42) accurately predicts the sideband noise-to-carrier ratio, not least because there are no parameters used in the calculation of (42) that have not been independently verified by measurement to the desired accuracy first. Since the relationship between an injected current and measured voltage

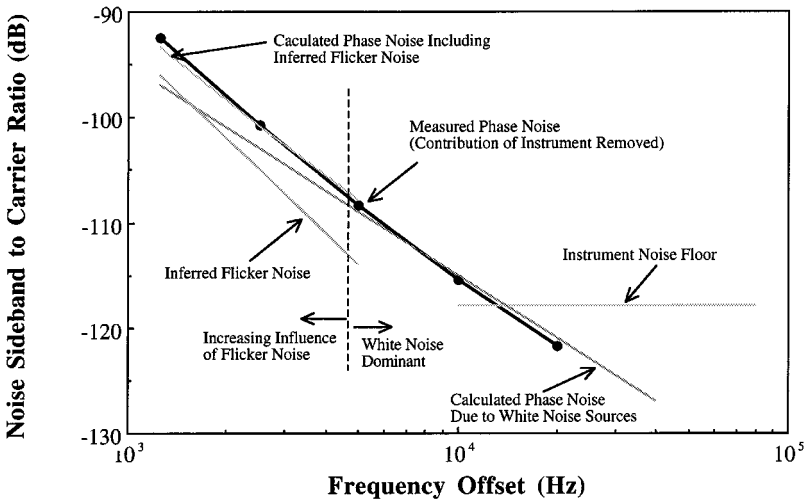

Fig. 14. Calculated and measured phase noise for the oscillator in Fig. 9.

response has also been accurately verified in the previous section, the significance of the measurement in Fig. 14 lies in verifying (35) and (36), as well as the power spectral densities of all the white noise sources in the oscillator, especially that of $M1$. Fig. 15 shows a measured spectrum of the oscillator.

In addition to having been derived on a rigorous basis, (42) is completely based on circuit parameters known to the designers. This makes it possible to derive a complete design procedure for the optimization of a Colpitts oscillator for RF applications. Due to limitation in space this discussion is not included here. It is, however, interesting to compare (42) or (43) to the well-known Leeson's formula, which designers have been using for the last 30 years, to examine the dependence on the resonator's quality factor Q in particular. In Leeson's original paper, the signal level P_s at the input of the active device is not very clearly defined, so that it can either be interpreted as the square of the oscillation voltage, or the power dissipated by the resonator. In the former case we can see that for a constant oscillation voltage, the noise to carrier ratio will only scale with the noise power given in (41), which clearly does not scale with Q^2. In the latter case, $P_s = (C_1/C_2)g_{mc}(V_m)^2/2$. Equation (43) can thus be rewritten as

$$\begin{aligned} S_{N/C}^{\Delta\omega} &= \frac{2\cdot V_n^2(\omega_o+\Delta\omega)}{(C_1/C_2)g_{mc}V_m^2}\left(\frac{C_1}{C_2}\right)g_{mc} \\ &= \frac{2kT}{(Q)^2P_s}\left(\frac{\omega_o}{2\Delta\omega}\right)^2\left(\frac{C_1}{C_2}\right) \\ &\quad\cdot\left[\gamma\frac{g_{mB}}{g_{mc}}+\left(\frac{C_2}{C_1}\right)^2+\gamma\frac{g_{mo}}{g_{mc}}\sqrt{\frac{\cos^{-1}(x)}{\pi}}\right] \\ &= \frac{2kTF}{(Q)^2P_s}\left(\frac{\omega_o}{2\Delta\omega}\right)^2 \end{aligned} \tag{44}$$

which is apparently Leeson's formula with an inverse dependence on Q^2! Closer examination of (44), however, shows that both the signal power P_s and the noise figure F so defined, far from being independent parameters, are usually also strong functions of Q. No conclusions could therefore really be drawn about the Q dependence of the oscillator noise performance on the basis of Leeson's formulation.

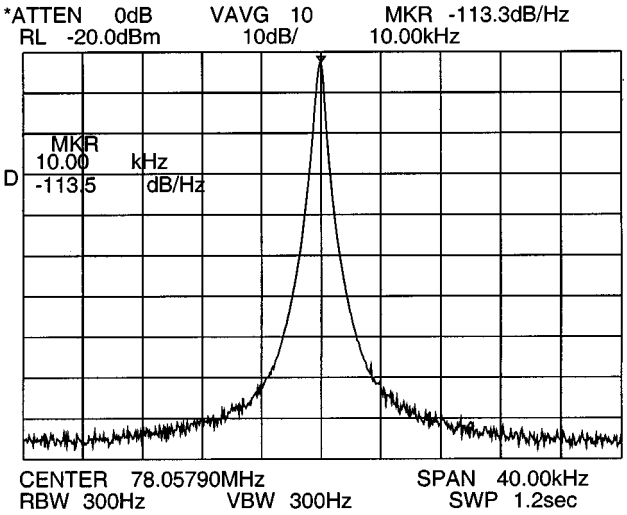

Fig. 15. Measured output power spectrum for the oscillator in Fig. 9.

In practical situations, one does sometimes find that doubling the Q of the tank improves the $S_{N/C}^{\Delta\omega}$ by exactly 6 dB, while the transistor and its bias current are unchanged. This can arise when the change of Q is purely due to improvement in the loss resistance R_s and that the middle term in the square brackets of (43) is much smaller than the other two terms. This may have been the case especially for designers using discrete MOSFET's or BJT transistors, where the transconductance for a given current is not within the designer's control. For an integrated circuit designer this need not be so, because the size of the transistor should be scaled down with g_{mc} to maintain just the necessary g_{mo}/g_{mc} range of 3–5 as explained earlier. In this case the noise factor F in Leeson's formulation is unchanged, while the signal power P_s has doubled. The improvement of $S_{N/C}^{\Delta\omega}$ will be 9 dB each time Q is doubled by halving R_s [29], [37].

On the other hand, $S_{N/C}^{\Delta\omega}$ can be significantly changed by different combinations of tank parameters with the same quality factor Q. Assuming a typical case, for example, that the loss resistance R_s of the inductor dominates the loss of the tank and scales linearly with the inductance L_s. Doubling the inductance and halving the capacitances therefore leaves both the Q

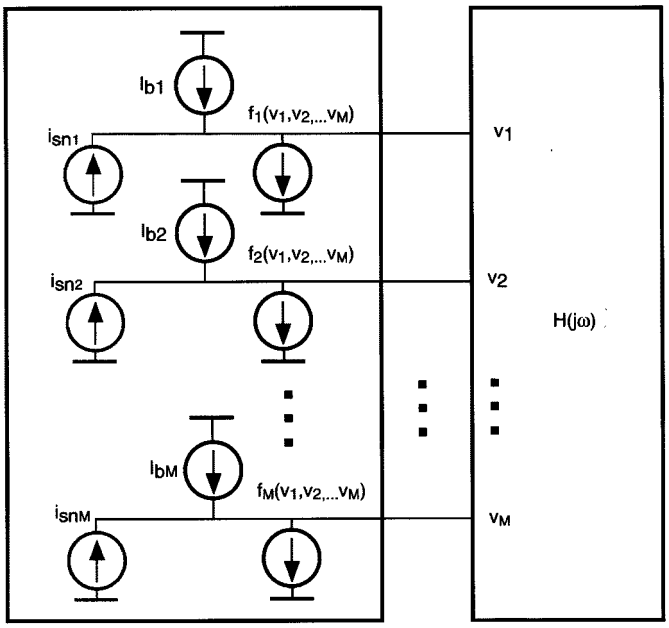

Fig. 16. Model of an arbitrary oscillator.

of the tank and its resonance frequency unchanged. The combined change in resistance and capacitance, however, causes g_{mc} in (43) to be halved, as well as the required g_{mo}, so that 3 dB can be gained either in achievable $S_{N/C}^{\Delta\omega}$ or in the required current consumption without improving the quality of the inductor! Indeed, we note that most recently published oscillators with integrated inductors have very small capacitors, which gave them respectable phase noise performance at a reasonable current consumption, even though the integrated inductors continue to have a poor quality factor of between three–six at 1 GHz. One's ability to improve phase noise by reducing capacitance, however, is limited by the parasitic capacitors associated with the circuit, which have higher losses and which tend to increase the required tuning range for the desired frequency. A higher tuning range in capacitance may also result in higher variability of oscillation amplitude, which in turn affects noise to carrier ratio.

An additional advantage of the phase noise model by (42) is that the role of current consumption (as opposed to power consumption P_{DC}, or the signal power P_s) is explicitly stated. Indeed, there is an almost one-to-one relationship between $S_{N/C}^{\Delta\omega}$ and bias current l_o. This point is important in RF oscillator designs for mobile communications, where power consumption is extremely important [38], [39].

V. General Formulation for LC Oscillator Analysis

From the discussion in Sections II and III, it should already be clear that the analysis on the Colpitts oscillator is applicable to most well-known LC oscillators. Since the vast majority of such oscillators effectively employ a single LC resonator, the topological differences lie in the different resonator (tapping) nodes from which the active devices are driven and to which the latter's currents are fed back, and indeed the number of active devices driving the circuit. Such oscillators share a basic characteristic that is the Class-C operation of the active devices. The voltage as well as current variables in steady state will still be periodic so that Fourier series expansion can be applied to extract the harmonics and dc bias and oscillation amplitude can still be determined by balancing the currents at feedback nodes. With high Q resonators the voltages on different resonator nodes will be sinusoidal, but the currents fed back from the active devices will be in pulses. The notion that the gating of active devices creates image components and such components interact with the response at the original interferences through an effective feedback is still valid, so that the exact characteristics of the active devices are unimportant in the noise part of the analysis. Since any excess gm will be canceled by the negative feedback, the inverse dependence of the interference response on the offset frequency will still hold, as does the odd symmetry between the pair of sidebands at low-offset frequencies. In a low-Q oscillator the harmonics of a resonator voltage cannot be neglected, so that more unknown variables are associated with the harmonics where more equations can be set up to solve them. Once the steady-state solutions are known, however, the equations for small interference responses will still be linear and readily solvable.

In the extreme case of an arbitrary passive network driven by an arbitrary number of active devices, the solution can also be formulated, assuming that the active devices are arbitrary voltage controlled current sources, as shown in Fig. 16. There are M voltage variables, represented by vector $\boldsymbol{v}$ controlling M effective active devices denoted by vector $\boldsymbol{f}$. The network is biased by M current sources $\boldsymbol{I_B}$.

$$\boldsymbol{v}(t) = [v_1(t)v_2(t)\cdots v_M(t)] \tag{45}$$

$$\boldsymbol{I}_B = [I_{b1}I_{b2}\cdots I_{bM}] \tag{46}$$

$$\boldsymbol{f}(t) = [f_1(t)f_2(t)\cdots f_M(t)]. \tag{47}$$

To account for discontinuities in $\boldsymbol{f}$, such as the piecewise characteristic of an FET, up to K pieces of gating functions can be defined for each component in $\boldsymbol{f}$, as shown in (48) at the bottom of the next page, where $\boldsymbol{g}(t)$ is a matrix of gating functions and $\boldsymbol{f_g}(t)$ are differentiable functions representing segments of $\boldsymbol{f}(t)$.

In steady state, the nodal voltages $\boldsymbol{v}$ are periodic. Therefore $\boldsymbol{f}$ is also periodic in time. Both can be represented with a Fourier series with the coefficient of the nth harmonic given by

$$\boldsymbol{V}(jn\omega_o) = \frac{\omega_o}{2\pi}\int_{-(\pi/\omega_o)}^{(\pi/\omega_o)} \boldsymbol{v}(t)\cdot e^{-jn\omega_o t}\,dt \tag{49}$$

$$\boldsymbol{F}(jn\omega_o) = \frac{\omega_o}{2\pi}\int_{-(\pi/\omega_o)}^{(\pi/\omega_o)} \boldsymbol{f}(t)\cdot e^{-jn\omega_o t}\,dt \tag{50}$$

where $n = 0, 1, 2, \cdots N$. Although in theory N can be arbitrarily high, in practical oscillators the selectivity of the passive RLC network rapidly reduces the higher harmonics in $\boldsymbol{v}$ to negligible levels relative to the fundamental component at $n = 1$. Assuming N is a finite (and most likely small) integer above

which $|\boldsymbol{V}(jn\omega_o)|$ is negligible, then Kirschhoff's current law (KCL) can be applied to each of the network's M nodes at dc as well as at all the N harmonics of $\boldsymbol{v}$ and $\boldsymbol{f}$. At dc

$$\boldsymbol{F}(0) = \boldsymbol{I}_B \tag{51}$$

whereas at the nth harmonic

$$\boldsymbol{V}(jn\omega_o)\cdot\boldsymbol{Y}(jn\omega_o) + \boldsymbol{F}(jn\omega_o) = 0. \tag{52}$$

In (52) the M by M matrix $\boldsymbol{Y}(jn\omega_o)$ is the admittance matrix of the passive network at the nth harmonic of the oscillation. From (51) and (52) the unknown vectors $|\boldsymbol{V}(jn\omega_o)|$ can be solved, either analytically or numerically.

To study the effect of a small interfering signal on the steady-state oscillation, we apply a small sinusoidal current to each node, as shown by the lightly shaded parts in Fig. 16, at an offset frequency $\Delta\omega$ of each harmonic n, $n = 0, 1, 2, \cdots N$ and $\Delta\omega < \omega_o/2$. Flicker noise can therefore also be analyzed, as shown in (53) at the bottom of the page. Expanding both the voltage $\boldsymbol{v}$ and the current vector into a Taylor series $\boldsymbol{f}$ (by first expanding $\boldsymbol{f_g}$, which is differentiable, before multiplying by the gating function) and neglecting the second- and high-order terms for small interferences, we can focus on the two sidebands around each harmonic as a result of modulation by the gating functions. Trigonometry can be used to collect systematically all individual terms of voltage perturbation $\Delta\boldsymbol{v}$ in the current perturbation $\Delta\boldsymbol{f}$ at the upper and lower sidebands of each harmonic. Having neglected higher order terms, the relations between $\Delta\boldsymbol{v}$, $\Delta\boldsymbol{f}$ and $\boldsymbol{I_{sn}}$ is linear, so that linear transfer functions and equations can be defined. Denoting

$$\begin{aligned}&\Delta\boldsymbol{V}_u[j(n\omega_o+\Delta\omega)]\\&\quad=[\,V_{u1n}\cdot e^{j\theta_{u1n}}\quad\cdots\quad V_{uMn}\cdot e^{j\theta_{uMn}}\,]\end{aligned} \tag{54}$$

$$\begin{aligned}&\Delta\boldsymbol{V}_l[j(n\omega_o-\Delta\omega)]\\&\quad=[\,V_{l1n}\cdot e^{j\theta_{l1n}}\quad\cdots\quad V_{lMn}\cdot e^{j\theta_{lMn}}\,]\end{aligned} \tag{55}$$

$$\begin{aligned}&\Delta\boldsymbol{F}_u[j(n\omega_o+\Delta\omega)]\\&\quad=[\,F_{u1n}\cdot e^{j\theta_{Fu1n}}\quad\cdots\quad F_{uMn}\cdot e^{j\theta_{FuMn}}\,]\end{aligned} \tag{56}$$

$$\begin{aligned}&\Delta\boldsymbol{F}_l[j(n\omega_o-\Delta\omega)]\\&\quad=[\,F_{l1n}\cdot e^{j\theta_{Fl1n}}\quad\cdots\quad F_{lMn}\cdot e^{j\theta_{FlMn}}\,]\end{aligned} \tag{57}$$

$$\begin{aligned}&\boldsymbol{I}_{sn}[j(n\omega_o+\Delta\omega)]\\&\quad=[\,I_{sn1}\cdot e^{j\theta_{sn1}}\quad\cdots\quad I_{snM}\cdot e^{j\theta_{snM}}\,]\end{aligned} \tag{58}$$

we can now relate the $2M(N+1)$ unknown response voltages in (54) and (55) to the interfering current sources in (58) and establish $2M(N+1)$ nodal current equations at the upper and lower sidebands, respectively

$$\begin{aligned}&\Delta\boldsymbol{V}_u[j(n\omega_o+\Delta\omega)]\cdot\boldsymbol{Y}[j(n\omega_o+\Delta\omega)] + \boldsymbol{F}_u[j(n\omega_o+\Delta\omega)]\\&\quad=\boldsymbol{I}_{sn}[j(n\omega_o+\Delta\omega)],\qquad n=0,\,1,\,2,\,\cdots N\end{aligned} \tag{59}$$

$$\begin{aligned}&\Delta\boldsymbol{V}_l[j(n\omega_o-\Delta\omega)]\cdot\boldsymbol{Y}[j(n\omega_o-\Delta\omega)] + \boldsymbol{F}_l[j(n\omega_o-\Delta\omega)]\\&\quad=0\qquad n=0,\,1,\,2,\,\cdots N.\end{aligned} \tag{60}$$

Note that (30) and (31) are linear in terms of the real and imaginary parts of the unknowns in (54) and (55). Once the unperturbed oscillation has been solved by solving equations (51) and (52) either analytically or numerically, equations (59) and (60) are solvable analytically, using standard linear algebra.

In order to apply the results we derived in the previous sections to signal-dependent noise sources, we seek to find an equivalent (signal-independent) noise source that has the same psd as the real noise source it represents for a given pattern of oscillating voltage or current in time. The first step in finding the equivalent is to define K noise sources $n'_{mk}(t)$ for each current-dependent noise source $n_m(t)$. If the average current during the kth time interval, during which $g_{mk}(t) = 1$, $t_{k-1}+iT < t \le t_k+iT$, $(i = 1, 2, \cdots$ and $T = 2\pi/\omega_o)$ is I_{mk} and the psd of n'_{mk} is the same as that of n_m for a constant bias of I_{mk}, $N_m(\omega, I_{mk})$, then $n_m(t)$ can be approximately represented by $n'_{mk}(t)$ during the same time interval. Putting all K intervals together we have

$$\begin{aligned}n_m(t) &\approx \sum_{k=1}^{K} n'_{mk}(t)g_{mk}(t) = \sum_{k=1}^{K} n'_{mk}(t)\\&\quad\cdot\left(\alpha_{mk} + \frac{2}{\pi}\sum_{i=1}^{\infty}\frac{1}{i}\,\sin(i\pi\alpha_{mk})\cos(i\omega_o t)\right)\end{aligned} \tag{61}$$

where $\alpha_{mk} = (t_k - t_{k-1})/T$. Assuming the $n'_{mk}(t)$'s are uncorrelated with one another, then [40]

$$\begin{aligned}N_m(\omega) \approx \sum_{k=1}^{K}&\\&\cdot\left[\alpha_{mk}^2 N(\omega, I_{mk}) + \left(\frac{1}{\pi}\right)^2\sum_{i=-\infty}^{\infty}\right.\\&\left.\cdot N(\omega - i\omega_o, I_{mk})\cdot\left(\frac{\sin(i\pi\alpha_{mk})}{i}\right)^2\right].\end{aligned} \tag{62}$$

$$\boldsymbol{f}(t) = \mathbf{diag}(\boldsymbol{g}(t)\cdot\boldsymbol{f}_g(t)) = \left[\sum_{k=1}^{K} g_{1k}(t)\cdot f_{gk1}(t)\quad\sum_{k=1}^{K} g_{2k}(t)\cdot f_{gk2}(t)\quad\cdots\quad\sum_{k=1}^{K} g_{Mk}(t)\cdot f_{gkM}(t)\right]. \tag{48}$$

$$\boldsymbol{i}_{sn} = [\,I_{sn1}\cdot\cos((n\omega_o+\Delta\omega)t+\theta_{sn1})\quad\cdots\quad I_{snM}\cdot\cos((n\omega_o+\Delta\omega)t+\theta_{snM})\,]. \tag{53}$$

In the case of white noise, the approximation of [35] can be applied, as in the derivation of (39), to obtain simple expressions of equivalent noise source psd.

VI. Conclusion

This paper has sought to overcome one of the major shortcomings of many existing papers on phase noise, which is to embed the conclusion of phase noise in the fundamental (starting-point) assumption of an analysis. A CMOS Colpitts oscillator is used as an example to illustrate the fundamental mechanism of additive noise to phase noise conversion. The active device in a well-designed oscillator operates in Class-C mode. The switching action of the active device modulates the interfering signal, so that DSB signals result for an SSB input. The interaction between the upper and lower sideband responses forms a feedback loop, and stability of the oscillation dictates that the feedback be negative, which is achieved when the image sideband becomes opposite in sign to the signal at the original sideband. The balance of current at the two frequencies also dictates that the two responses are equal in amplitude. The resulting odd symmetry in the power spectrum is the same as that of a phase modulated signal. The negative feedback loop will be effectively broken when the offset frequency is too far away from the carrier, so that the transimpedance of the resonator is too low to maintain the link between modulated current and gate voltage. In this case, the response is that of the resonator alone and no conversion to phase noise takes place. The details of the transistor and the passband width of the resonator are otherwise unimportant, except in determining the crossover frequency between conversion to phase and no conversion.

Noise sources associated with a switching transistor are affected by the duty cycle in which the latter conducts current. This has been taken into account in this paper in the identification of all white noise sources in the Colpitts oscillator.

Exact expression for the steady-state amplitude of a CMOS Colpitts oscillator has also been derived here. Prediction of amplitude is therefore made independent of simulation and much easier. An analytical expression of amplitude, together with the analytical expression of phase noise, allows an analytical expression of noise to carrier ratio to be established, that is completely described by circuit parameters and contains no intermediate variables. The influence of the LC resonator quality factor, bias current, value of capacitances, as well as the transistor's transconductance coefficient on the N/C ratio, respectively, is explicit.

Controlled experiments have been carefully devised to verify the theory derived in the paper. The predicted oscillation amplitude is consistently within 1 dB of measurements. The predicted duty cycle also matches measured values by the same accuracy. The oscillator response (as well as its image) to an injected interfering current agrees with what the theory predicts within the accuracy with which parameters of the passive tank can be measured. At an 80–MHz range, this accuracy is better than 1 dB. The crossover frequency between phase and additive noise and indeed its very existence have been confirmed by experiments.

Measurements on phase noise to carrier ratio also show that the agreement with the formula derived in this paper is within 1 dB, the repeatability of any phase noise measurement and the accuracy with which circuit parameters have been independently measured. The phase noise model in this paper can therefore be used in practical designs with confidence.

A general formulation for the analysis of arbitrary oscillators has been outlined in this paper, in the spirit of the Colpitts oscillator analysis. The conclusions of the latter analysis, however, should apply to most existing LC oscillators, as the important mechanisms in the conversion to phase noise are largely independent of the exact construction of an LC oscillator.

References

[1] I. L. Berstein, "On fluctuations in the neighborhood of periodic motion of an auto-oscillating system," *Doklady Akad. Nauk.*, vol. 20, p. 11, 1938.

[2] A. Spälti, "Der einfluss des thermischen widerstandsrauschens und des schrotteffectes auf die stormodulation von oscillatoren," *Bulletin Schweizerischen Electrotechnischen Vereins*, vol. 39, pp. 419–427, June 1948.

[3] A. Blaquiére, "Spectre de puissance d'un oscillateur nonlinéaire perturbé par le bruit," *Ann. Radio Elect.*, vol. 8, pp. 153–179, August 1953.

[4] Hafner, "The effect of noise in oscillators," *Proc. IEEE*, vol. 54, pp. 179–198, Feb. 1966.

[5] A. van der Ziel, *Noise in Solid-State Devices and Circuits*. New York: Wiley-lnterscience, 1986.

[6] D. B. Leeson, "A simple model of feedback oscillator noise spectrum," *Proc. IEEE*, pp. 329–330, Feb. 1966.

[7] G. Sauvage, "Phase noise in oscillators: A mathematical analysis of Leeson's model," *IEEE Trans. Instrum. Meas.*, vol. IM-26, Dec. 1977.

[8] W. Robins, *Phase Noise in Signal Sources*. London: Peter Peregrinus Ltd, 1982.

[9] J. Everard, "Low-noise power-efficient oscillators: Theory and design," *Proc. Inst. Elect. Eng.*, pt. G, vol. 133, pp. 172–180, Aug. 1986.

[10] F. Kaertner, "Determination of the correlation spectrum of oscillators with low noise," *IEEE Trans. Microwave Theory Tech.*, vol. 37, pp. 90–101, Jan. 1989.

[11] J. Craninckx and M. Steyaert, "Low noise voltage-controlled oscillators using enhanced LC-tanks," *IEEE Trans. Circuits Syst.*, vol. 42, pp. 794–804, Dec. 1995.

[12] A. Hajimiri and T. Lee, "A general theory of phase noise in electrical oscillators," *IEEE J. Solid-State Circuits*, vol. 33, pp. 179–194, Feb. 1998.

[13] C. Samori and A. Lacaita, "Spectrum folding and phase noise in LC tuned oscillators," *IEEE Trans. Circuits Syst.*, vol. 45, pp. 781–790, July 1998.

[14] N. Nguyen and R. Meyer, "A 1.8-GHz monolithic LC voltage-controlled oscillator," *IEEE J. Solid-State Circuits*, vol. 27, pp. 444–450, March 1992.

[15] ——, "Si IC-compatible inductors and LC passive filters," *IEEE J. Solid-State Circuits*, vol. 25, pp. 1028–1031, Aug. 1990.

[16] P. Basedau and Q. Huang, "A 1GHz, 1.5V monolithic LC oscillator in 1-μm CMOS," in *Proc. 1994 European Solid-State Circuits Conf.*, Ulm, Germany, Sept. 1994, pp. 172–175.

[17] M. Soyuer *et al.*, "A 2.4-GHz silicon bipolar oscillator with integrated resonator," *IEEE J. Solid-State Circuits*, vol. 31, pp. 268–270, Feb. 1996.

[18] A. Ali and J. Tham, "A 900MHz frequency synthesizer with integrated LC voltage-controlled oscillator," in *ISSCC Dig. Technical Papers*, San Francisco, CA, Feb. 1996, pp. 390–391.

[19] A. Rofougaran *et al.*, "A 900MHz CMOS LC-oscillator with quadrature outputs," in *ISSCC Dig. Technical Papers*, San Francisco, , 1996, pp. 392–393.

[20] M. Soyuer *et al.*, "A 3V 4GHz nMOS voltage-controlled oscillator with integrated resonator," in *ISSCC Dig. Technical Papers*, San Francisco, CA, Feb. 1996, pp. 394–395.

[21] B. Razavi, "A 1.8GHz CMOS voltage-controlled oscillator," in *ISSCC Dig. Technical Papers*, San Francisco, CA, Feb. 1997, pp. 388–389.

[22] L. Dauphinee, M. Copeland, and P. Schvan, "A balanced 1.5GHz voltage controlled oscillator with an integrated LC resonator," in *ISSCC Dig. Technical Papers*, San Francisco, CA, Feb. 1997, pp. 390–391.

[23] J. Jansen *et al.*, "Silicon bipolar VCO family for 1.1 to 2.2GHz with fully-integrated tank and tuning circuits," in *ISSCC Dig. Technical Papers*, San Francisco, CA, Feb. 1997, pp. 392–393.
[24] J. Craninckx and M. Steyaert, "A 1.8GHz low-phase-noise CMOS VCO using optimized hollow spiral inductors," *IEEE J. Solid-State Circuits*, vol. 32, pp. 736–744, May 1997.
[25] ——, "A fully integrated spiral-LC CMOS VCO set with prescaler for GSM and DCS-1800 systems," in *Proc. Custom Integrated Circuit Conf.*, Santa Clara, , May 1997, pp. 403–406.
[26] J. Parker and D. Ray, "A low-noise 1.6GHz PLL with on-chip loop filter," in *Proc. CICC*, Santa Clara, CA, May 1997, pp. 407–410.
[27] M. Zannoth *et al.*, "A fully integrated VCO at 2GHz," in *ISSCC Dig. Technical Papers*, San Francisco, CA, Feb. 1998, pp. 224–225.
[28] P. Kinget, "A fully integrated 2.7V 0.35μm CMOS VCO for 5GHz wireless applications," in *ISSCC Dig. Technical Papers*, San Francisco, CA, Feb. 1998, pp. 226–227.
[29] Q. Huang, "Phase-noise-to-carrier ratio in LC oscillators," in *Circuits and Systems for Wireless Communications*, M. Helfenstein and G. S. Moschytz, Eds. Amsterdam, The Netherlands: Kluwer, 1999, ch. 7, pp. 75–107.
[30] D. Pederson and K. Mayaram, *Analog Integrated Circuits for Communication*. Boston, MA: Kluwer, 1991.
[31] Q. Huang, "Power consumption vs LO amplitude for CMOS colpitts oscillators," *Proc. CICC*, pp. 255–258, May 1997.
[32] ——, "Power consumption vs. LO amplitude for CMOS colpitts oscillators," *Proc. CICC (Lecture Presentation)*, pp. 255–258, May 1997.
[33] B. Razavi, Ed., *Monolithic Phase-Locked Loops and Clock Recovery Circuits*. Piscataway, NJ: IEEE, 1996.
[34] T. Lee, "Oscillator phase noise: A tutorial," in *Proc. CICC*, San Diego, CA, May 1999, pp. 373–380.
[35] J. Fischer, "Noise sources and calculation techniques for switched capacitor filters," *IEEE J. Solid-State Circuits*, vol. SC-17, pp. 742–752, Aug. 1982.
[36] Q. Huang and P. Basedau, "Design considerations for high-frequency crystal oscillators digitally trimmable to sub-ppm accuracy," *IEEE Trans. VLSI*, vol. 5, pp. 408–416, Dec. 1997.
[37] D. Pfaff and Q. Huang, "A quarter-mircron CMOS, 1GHz VCO/prescaler-set for very low power applications," in *Proc. CICC*, May 1999, pp. 629–652.
[38] S. Rogerson, "Where less is more," *Mobile Eur.*, vol. 7, pp. 27–30, Feb. 1997.
[39] Q. Huang *et al.*, "The impact of scaling down to deep submicron on CMOS RF circuits," *IEEE J. Solid-State Circuits*, vol. 33, pp. 1023–1036, July 1998.
[40] S. Haykin, *An Introduction to Analog and Digital Communications*. New York: Wiley, 1989.

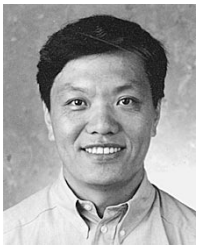

Qiuting Huang (S'86–M'88–SM'96) received the B.Sc. degree from the Department of Precision Instruments, Harbin Institute of Technology, Harbin, China, in 1982 and the Ph.D. degree from Departement Elektrotechniek, ESAT laboratories, Katholieke Universiteit Leuven, Heverlee, Belgium in 1987.

Between 1987 and 1992 he was a Lecturer at the University of East Anglia, Norwich, U.K. Since January 1993, he has been with the Integrated Systems Laboratory, Swiss Federal Institute of Technology, Zurich, Switzerland, where he is an Associate Professor. His general field of research is in analog and mixed analog–digital integrated circuits and systems. His current research projects include RF transceivers for wireless communications, low-power data converters, interface circuits to sensors and actuators, and low-noise low-power IC's for biomedical applications.